Observational evidence of a hemispheric-wide ice–ocean albedo feedback effect on Antarctic sea-ice decay

Sohey Nihashi[1] and Donald J. Cavalieri[2]

Received 19 December 2005; revised 26 June 2006; accepted 15 August 2006; published 2 December 2006.

[1] The effect of ice–ocean albedo feedback (a kind of ice-albedo feedback) on sea-ice decay is demonstrated over the Antarctic sea-ice zone from an analysis of satellite-derived hemispheric sea ice concentration and European Centre for Medium-Range Weather Forecasts (ERA-40) atmospheric data for the period 1979–2001. Sea ice concentration in December (time of most active melt) correlates better with the meridional component of the wind-forced ice drift (MID) in November (beginning of the melt season) than the MID in December. This 1 month lagged correlation is observed in most of the Antarctic sea-ice covered ocean. Daily time series of ice concentration show that the ice concentration anomaly increases toward the time of maximum sea-ice melt. These findings can be explained by the following positive feedback effect: once ice concentration decreases (increases) at the beginning of the melt season, solar heating of the upper ocean through the increased (decreased) open water fraction is enhanced (reduced), leading to (suppressing) a further decrease in ice concentration by the oceanic heat. Results obtained from a simple ice–ocean coupled model also support our interpretation of the observational results. This positive feedback mechanism explains in part the large interannual variability of the sea-ice cover in summer.

Citation: Nihashi, S., and D. J. Cavalieri (2006), Observational evidence of a hemispheric-wide ice–ocean albedo feedback effect on Antarctic sea-ice decay, *J. Geophys. Res.*, *111*, C12001, doi:10.1029/2005JC003447.

1. Introduction

[2] The Antarctic sea-ice zone has primarily a seasonal sea-ice cover, and most of the ice surface is covered by snow with a high albedo. In the seasonal and marginal ice zones, the existence of open water with an albedo much lower than that of sea ice results in high solar radiation absorption by the upper ocean during summer [*Maykut and McPhee*, 1995]. This absorption is the dominant heat source for bottom and lateral melting of the ice [*Maykut and Perovich*, 1987]. This process is particularly important for the Antarctic sea-ice covered ocean which has a relatively large open water fraction resulting from the divergent drift of ice.

[3] From the calculated net heat flux in the Arctic and Antarctic Oceans, surface melting of the sea-ice cover and the subsequent formation of meltponds appears to be small in the Antarctic, unlike that for the Arctic [*Andreas and Ackley*, 1982]. Multiple satellite data sets also indicate that areas of surface melting are sparse and short-lived in the Antarctic sea-ice zone [*Drinkwater and Liu*, 2000]. From a heat budget analysis of the Antarctic sea-ice zone, *Nihashi and Ohshima* [2001] showed that net heat input at the water surface from the atmosphere during the time of maximum melt (December) reaches 100–150 W m^{-2} as a result of solar heating, and is one or two orders of magnitude larger than the heat input at the ice surface ($\leq$ 10 W m^{-2}) because of the albedo difference. Further, they showed that the total heat input into the upper ocean through areas of open water is comparable to the latent heat of sea-ice decay for the entire Antarctic sea-ice zone.

[4] The heat input through open water is much larger than the estimated heat entrained from the deeper ocean, another possible heat source. In the Weddell Sea, the heat flux from the deeper ocean during winter was estimated to be about 20–50W m^{-2} due to the underlying warm Circumpolar Deep Water (CDW) [*Gordon and Huber*, 1990; *McPhee et al.*, 1999]. However, in summer, since the oceanic surface layer is strongly stratified both by heating and melting, entrainment of heat from the deeper ocean is suppressed. Further, winter water (WW) exists beneath the surface layer at a temperature near the freezing point and prevents the underlying warm CDW from reaching the surface. Also, from the Gordon and Huber study, the winter ocean heat flux was estimated to be 41 W m^{-2} and the annual value was estimated to be 16 W m^{-2}; thus, the summer value is expected to be small. Based on a heat budget analysis, *Nihashi and Ohshima* [2001] showed that an assumed spatially uniform flux of 10 W m^{-2} from the deeper ocean is less than 25% of the total heat input through open water

[1] Institute of Low Temperature Science, Hokkaido University, Sapporo, Japan.
[2] Hydrospheric and Biospheric Sciences Laboratory, NASA Goddard Space Flight Center, Greenbelt, Maryland, USA.

0148-0227/06/2005JC003447

from the atmosphere during the active melt period (December–January). Ignoring the deeper ocean heat flux appears to be valid during the active melt season as a first-order approximation. Therefore, in the summer Antarctic sea-ice zone, heat input into the ice–upper ocean system mainly occurs over the open water areas and this heat input is the main heat source for sea-ice decay.

[5] If sea ice is primarily melted by heat input into the upper ocean through open water areas within the ice pack, the following positive feedback mechanism is possible in the ice–upper ocean coupled system: once ice concentration decreases (increases) at the beginning of the melt season, heat input into the upper ocean through the increased (decreased) open water fraction is enhanced (reduced), leading to (suppressing) a further decrease in ice concentration through ice melting by the oceanic heat. This effect is regarded as a kind of 'ice-albedo feedback', because the difference in surface albedo between ice and water causes the feedback.

[6] The term of 'ice-albedo feedback' for sea ice is often used for the following positive feedback mechanism: a decrease in the surface albedo of snow/ice due to surface melt with melt pond formation causes an increase in the solar radiation absorption, and then this causes further surface melt and a further surface albedo decrease [e.g., *Curry et al.*, 1995]. On the other hand, the positive feedback mechanism described in the previous paragraph is caused by the areal albedo change due to a change in open water fraction rather than a change in the surface albedo of snow/ice. In this study, to avoid misunderstanding, we use hereafter the term of 'ice–ocean albedo feedback' for the albedo feedback effect caused by a change in open water fraction within the ice pack. Since the surface melting appears to be small in the Antarctic sea-ice zone, the ice-albedo feedback effect caused by a change in the surface albedo of snow/ice is expected to be small.

[7] *Ackley et al.* [2001] applied the ice–ocean albedo feedback mechanism ('open water–albedo feedback' in their study) to the Ronne polynya during the 1997/98 summer season; the anomalously large open water area was initiated by an anomalous divergent wind field. They concluded that the open water area was enhanced through this feedback mechanism. A numerical modeling study also supported this idea [*Hunke and Ackley*, 2001]. For the 25–45°E sector, *Ohshima and Nihashi* [2005] demonstrated this feedback effect using a simple two-dimensional ice–ocean coupled model for the case of meridional ice retreat. Since the heat input mainly occurs over open water and this heat input is the main heat source for sea-ice decay, the ice–ocean albedo feedback effect is expected to be particularly prominent for the entire Antarctic sea-ice zone. Although this kind of albedo feedback effect is thought to be important in the Antarctic sea-ice zone, there have been very few studies that show the existence of this feedback mechanism from observational data, except for some specific regions. The objective of this study is to demonstrate through an analysis of observational data sets the ice–ocean albedo feedback effect on sea-ice decay over the entire Antarctic sea-ice zone.

[8] The organization of the paper is as follows. Section 2 describes the data used in the study, our method is explained in section 3, and the results and discussion are presented in section 4. A summary is given in section 5.

2. Data

[9] In this study a 22-year (1979–2001) daily sea ice concentration data set, previously derived from the Scanning Multichannel Microwave Radiometer (SMMR) on the Nimbus-7 satellite (1979–1987) and the Special Sensor Microwave Imager (SSM/I) on the Defense Meteorological Satellite Program (DMSP) F8, F11, and F13 satellites (1987–2001) [*Cavalieri et al.*, 1999] using the NASA Team algorithm [*Cavalieri et al.*, 1984; *Gloersen and Cavalieri*, 1986; *Cavalieri et al.*, 1991, 1995], is employed. The spatial resolution of the ice concentration maps is ~25 km. The ice edge is defined as the 15% ice concentration contour. All late spring periods (November–December) from 1979 through 2001 are used except for 1987 when a 6-week period (December 1987–mid January 1988) of SSM/I data were missing.

[10] Air temperatures at 2 m, dew point temperatures at 2 m, wind at 10 m, and surface sea level pressures (SLP) are obtained from the European Centre for the Medium-Range Weather Forecasts Re-Analysis (ERA-40) data set for the same period as the ice concentration data. The resolution is $1.125° \times 1.125°$. We use daily data averaged at 0000 UT, 0600 UT, 1200 UT, and 1800 UT. For cloud cover, we use the International Satellite Cloud Climatology Project (ISCCP) D2 data with a resolution of $2.5° \times 2.5°$. We averaged the monthly cloud cover from 1983 to 2001 to obtain a climatological data set. The cloud data are used for the heat budget calculation in section 4.

[11] We use the monthly mean ice motion data retrieved from the SMMR and SSM/I [*Schmitt et al.*, 2004]. All November data during 1979–1997 except for 1987 are used. The spatial resolution of the ice motion maps is ~100 km. The accuracy of large-scale Antarctic ice motion retrievals from passive microwave data has been determined through quantitative comparisons with drifting buoys [*Kwok et al.*, 1998; *Drinkwater and Liu*, 1999; *Drinkwater et al.*, 1999]. During late spring (December) and summer (January and February), the period we focus on in this study, ice motion retrievals from passive microwave data are unreliable because of the decorrelation of the passive microwave data resulting from rapid sea-ice decay and atmospheric interference [*Kwok et al.*, 1998]. Therefore, we mainly use ice drift derived from SLP in addition to the satellite-retrieved ice drift since sea-ice drift is forced predominantly by the geostrophic wind determined from the SLP pattern [*Kwok et al.*, 1998; *Drinkwater*, 1998; *Drinkwater and Liu*, 1999; *Drinkwater et al.*, 1999]. In this study, the wind-forced ice drift is calculated from the geostrophic wind based on SLP, where the ice drift is assumed to be 1.5% of the wind speed and directed 18° to the left [*Thorndike and Colony*, 1982; *Vihma et al.*, 1996; *Kottmeier and Sellmann*, 1996; *Uotila et al.*, 2000]. In order to check the accuracy of the ice drift derived from SLP, a comparison with the ice drift retrieved from satellite data in November when the ice drift derived from satellites is thought to be relatively reliable is given in Appendix A.

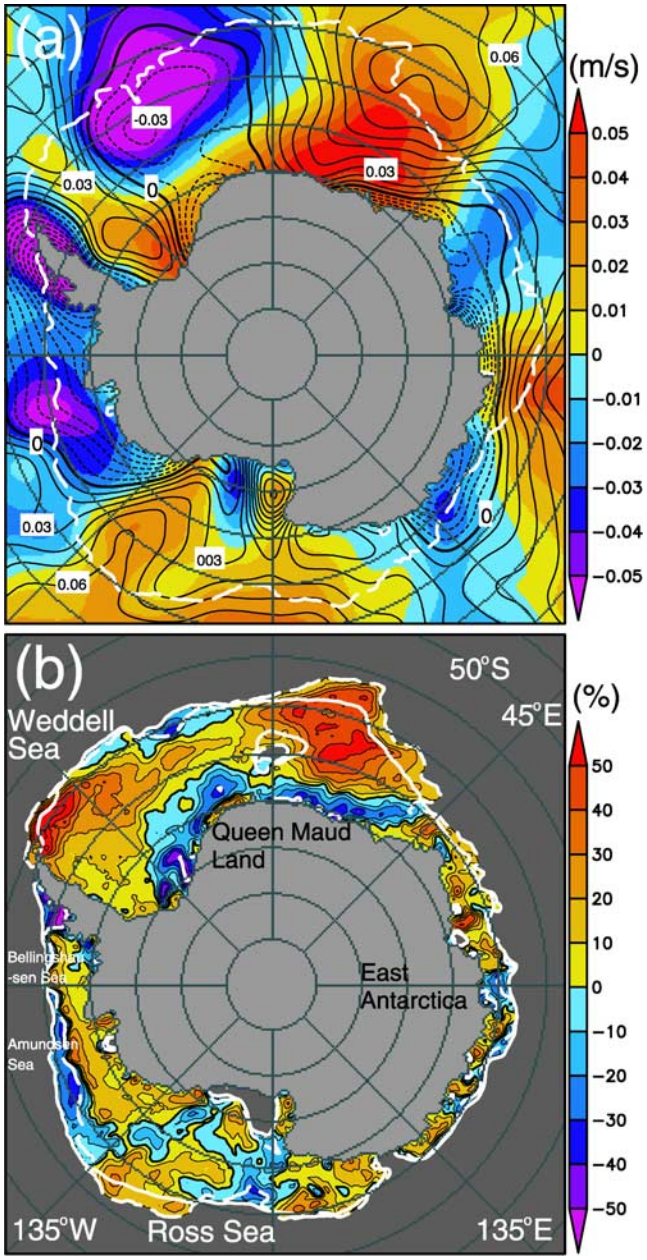

Figure 1. (a) MID calculated from SLP and the anomalies for November 1988. Contours and shades denote the MID and the anomalies, respectively. The contour interval is 0.01 m s^{-1}. Positive values indicate northward drift. MID and the anomaly are interpolated on the ice concentration grid. The white dashed line indicates ice edge in November 1988. (b) Mean monthly ice concentration anomalies for December 1988. The counter interval is 10%. The white dashed line and the white solid line indicate the ice edge in December 1988 and the climatological ice edge in December averaged from 1979 to 2001, respectively.

[12] Analyses are made on the SMMR and SSM/I grid. Thus, the ice drift data and the atmospheric data are interpolated onto the SMMR and SSM/I grid using a Gaussian weighting function, except for the comparison shown in Appendix A. For the Appendix A comparison, ice drift derived from SLP is interpolated onto the satellite derived ice motion grid.

3. Method

[13] The beginning of the melt season is characterized by relatively little freezing and melting, so that an initial change in ice concentration (or open water fraction) is caused mainly by ice drift as a result of wind forcing. Thus, in this study we first compare the ice drift at the beginning of the melt season with ice concentration during the most active melt season using monthly averaged data. November is regarded as the beginning of the melt season, because it is the time when the net heat input at the water surface becomes positive for most of the sea-ice zone and when the retreat of the sea-ice cover begins [*Nihashi and Ohshima*, 2001]. December is regarded as the most active melt season, because the net heat input at the water surface is largest and the retreat of the sea-ice cover is fastest.

[14] From the comparison of ice drift data derived from SLP and from satellites (Appendix A), the positive and negative patterns of ice drift as calculated from SLP appear to be fairly reliable, but the accuracy of its speed is poor. Because of the comparative results shown in Appendix A, we mainly focus on the coastal region around Antarctica and use the meridional component of ice drift (hereafter MID) because the relationship between ice drift and ice concentration appears to be most robust: northward (southward) advection of ice will cause divergence (convergence) in the coastal region due to the influence of the fixed continental boundary.

[15] Next, we examine whether the initial change in ice concentration increases during the melt season using both 10-day mean and daily data. The result from an analysis of these data is that there is an increase in the ice concentration change on average during the melt season which we interpret as the result of the ice–ocean albedo feedback effect. Finally, this interpretation is confirmed quantitatively by performing model runs using a simple ice–ocean coupled model both with and without this feedback mechanism.

4. Results and Discussion

[16] The MID calculated from SLP and the MID anomaly both for November 1988 are shown in Figure 1a. The monthly anomalies are constructed by subtracting the 22-year climatological monthly means from the monthly means of individual years. The MID derived from satellite data and the anomaly show similar distributions (not shown here). An anomaly map of ice concentration for the following December is shown in Figure 1b. These anomalies are constructed in the same way as the MID anomalies. In the coastal area of East Antarctica (50–85°E and 110–140°E) and the Amundsen and Bellingshausen Seas (75–140°W), both the November MID and the MID anomalies are negative (southward; Figure 1a). In these regions, the ice concentration anomalies for the following December are positive near Antarctica (Figure 1b), probably due to the southward ice drift in November. On the other hand, in the positive MID anomaly areas, especially the Weddell Sea (∼45°W), the coastal area of Queen Maud Land (0–25°E), and the eastern Ross Sea (∼150°W), where the MID is also

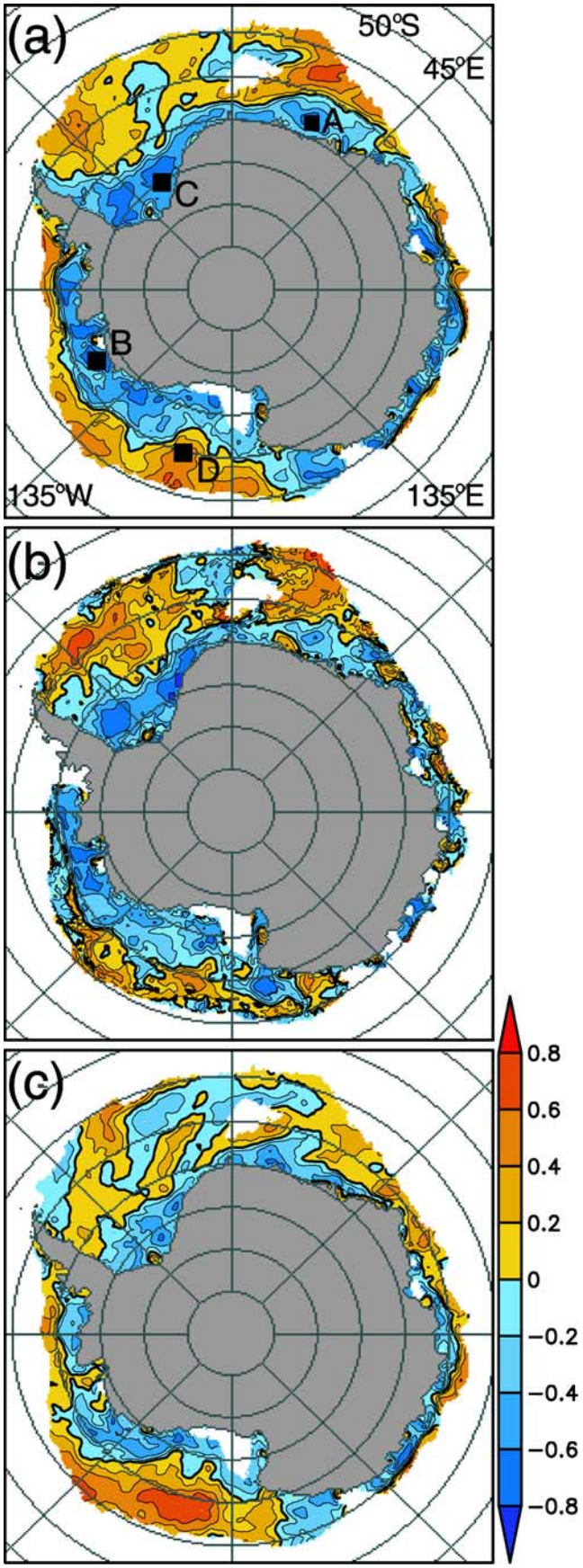

positive, the ice concentration anomalies are negative near Antarctica. Although these relationships are not clearly shown in some regions probably because of the complex coast lines and the MID distributions, the above mentioned relationships can be generalized by showing the correlation coefficients between the November MID and December ice concentration for all 22 years (Figure 2a). The correlations are generally negative near Antarctica. Similar results are obtained even if we use the November MID retrieved from the satellite data (Figure 2b).

[17] The correlation coefficients between the ice concentration and the MID calculated from SLP are also examined using daily data for the 22 Novembers (not shown here). The results show a similar relationship as in Figure 2a, but it is also shown by a lag-correlation analysis that the relationship disappears after 2–3 days. This indicates that the ice concentration anomalies in December (Figure 1b) cannot be explained only by the November MID (Figure 1a) because its effect lasts only a few days.

[18] Although the sea ice responds to winds instantaneously ($\ll$ 1 month), the negative correlations near Antarctica between the December MID and December ice concentration are relatively weak (Figure 2c). In Figures 2a and 2c, grid points with correlations greater than 0.5 have a significance greater than 99%. For the case of Figure 2c (December MID versus December ice concentration), the number of grid points with significant negative correlation is $\sim$25% of those for the case of Figure 2a (November MID versus December ice concentration). This indicates that the December MID is not sufficient to determine ice concentration anomalies in December. Thus, Figures 2a and 2c imply that the ice concentration anomalies in December are mainly determined by the November MID rather than the December MID and that they are amplified possibly due to the ice–ocean albedo feedback effect.

[19] Next, to examine this in more detail, we select three points, A–C, in regions of high negative correlation (Figure 2a). Figures 3a–3c show the time series of November MID and December ice concentration for points A to C. The fact that the MID and ice concentration change randomly during the whole period (1979–2001) implies that the high correlations in Figure 2a do not arise from a trend-like feature or periodic variation [e.g., *White and Peterson*, 1996; *Venegas and Drinkwater*, 2001; *Venegas et al.*, 2001].

[20] Table 1 summarizes the mean ice concentration and the standard deviation at points A to C calculated every 10 days from early November to late December for the 22 years. Since the focus is on the seasonal timescale in this analysis, the ice concentration is spatially averaged using the surrounding 11 $\times$ 11 grid point data to reduce the advective effect of sea ice. The 11 grid points ($\sim$275 km)

Figure 2. Patterns of correlation coefficients between the MID and the ice concentration (IC). The correlations are calculated on the ice concentration grid. (a) The November MID calculated from SLP versus the December IC from 1979 to 2001. (b) The November MID retrieved from the satellites versus the December IC from 1979 to 1997. (c) The December MID calculated from SLP versus the December IC from 1979 to 2001. The contour interval is 0.2.

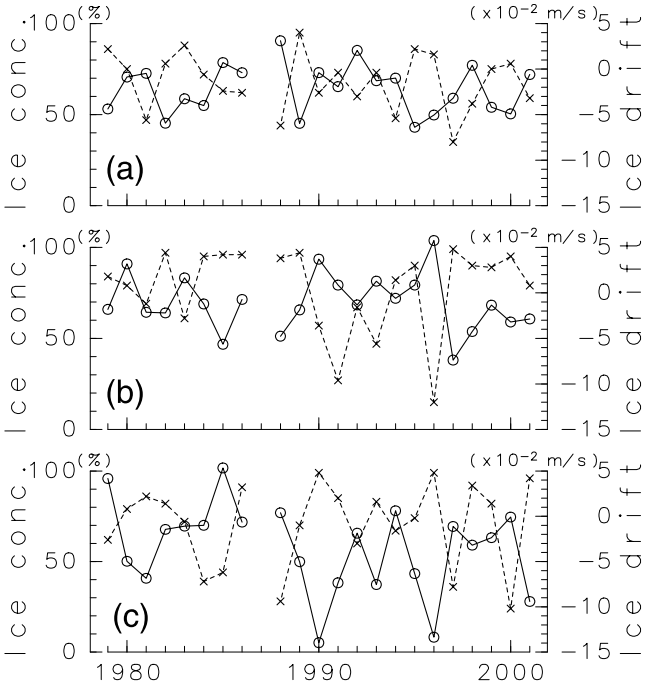

Figure 3. Time series of the November MID calculated from SLP (solid line with circles) and the ice concentration in December (dashed line with crosses) at points (a) A, (b) B, and (c) C. Their locations are indicated in Figure 2a.

correspond to a distance of ice drift during the two month period (November–December) when the speed is $\sim$0.05 m s^{-1} in the same direction. Table 1 shows that the standard deviation increases toward the time of maximum melt suggesting that the ice concentration variations increase.

[21] In order to show whether the ice concentration anomalies at the beginning of the melt season actually increase during the active melt period, daily time series of ice concentration during November–December of each year is also examined at points A to C. Ice concentrations are spatially averaged in the same way as described in the above paragraph. Further, the ice concentrations are smoothed using an 11-day running mean because the focus is on the seasonal timescale. We select those years which best illustrate the ice–ocean albedo feedback scenario by using the following criteria: (1) The difference in ice concentration between an individual year and climatology (daily ice concentration averaged for 22 years) on December 31 is $\geq$10%. This is twice as large as the standard deviation at the beginning of the melt season (early November) which is thought to be caused by MID (Table 1). (2) The time series of the year doesn't cross the 22-year climatological average during December, that is, a state in which an ice concentration anomaly of a given sign in November remains throughout December. The years satisfying these criteria are called Case 1; all other years are called Case 2.

[22] Case 1 (Figures 4a–4c), demonstrates that the differences in ice concentration between a given year (black line) and climatology (gray line) generally increase from November through December. This ice concentration difference in December corresponds to the ice concentration anomaly shown in Figure 1b. For Point A, the average time series of years that are larger and smaller than the climatology are shown in Figure 5a. The daily standard deviations of both the larger and smaller years averaged for December are $\sim$8%. The differences between the averages and the climatology increase from the end of November (5–10%) through the end of December (25–30%; Figure 5b). For the case of the smaller ice concentration years, the increase in the difference is small when the ice concentration is small ($\leq$30%; dotted line in Figures 5a and 5b). The reason for this is discussed later. Similar results as those shown for Point A in Figures 5a and 5b are obtained for the other points.

[23] Case 2 (Figures 4d–4f) reveals that the time series of ice concentration of each year (black line) is similar to the climatology (gray line) or fluctuates around the climatology. The ice concentration anomalies for these years are small. The average time series for Case 2 is also very close to the climatology (not shown here). The daily standard deviation averaged for December is $\sim$9%, indicating that the interannual variability of Case 2 is generally smaller than the difference between the average time series of Case 1 and the climatology (Figure 5b).

[24] Table 2 summarizes the number of years for each case at each point. It is clear that Case 1 generally has more years for each point than Case 2. For the entire 22-year period, the area where the occurrence of Case 1 is greater than or equal to 50% is $\sim$60% of the entire Antarctic sea ice zone.

[25] These results are now examined quantitatively at point A using a simple ice–ocean coupled model in which sea-ice melting is caused by heat input through open water (proposed by *Ohshima and Nihashi* [2005]; see Appendix B). In East Antarctica corresponding to point A, *Ohshima and Nihashi* [2005] showed that sea-ice retreat is determined by the local heat balance to a first-order approximation using this simple model. The input parameters of this model are the oceanic surface mixed layer thickness (H), the average ice thickness (h_0), and the bulk heat transfer coefficient between ice and ocean (K_b). The forcing of this model is daily net heat input at the water surface (F_n). In this study, H is set to 25 m [*Gleitz et al.*, 1994; *Ohshima et al.*, 1998; *Vaillancourt et al.*, 2003; *Nihashi et al.*, 2005], and h_0 is set to 1 m [*Ohshima et al.*, 1998; *Strass and Fahrbach*, 1998; *Worby et al.*, 1998; *Timmermann et al.*, 2004; *Nihashi et al.*, 2005]. K_b is set to 1.2×10^{-4} m s^{-1} [*Nihashi et al.*, 2005;

Table 1. Temporal Change in 10-Day Mean Observational Ice Concentration and Net Heat Input at Water Surface at Points A–D, Averaged From 1979 to 2001, With Its Standard Deviation

	Point A	Point B	Point C	Point D
	Ice concentration (%)			
Early Nov	88 ± 4	87 ± 4	92 ± 4	87 ± 5
Mid-Nov	84 ± 5	85 ± 6	90 ± 5	86 ± 5
Late Nov	79 ± 6	81 ± 9	85 ± 10	84 ± 6
Early Dec	75 ± 8	77 ± 14	79 ± 15	77 ± 10
Mid-Dec	69 ± 15	74 ± 18	72 ± 20	66 ± 16
Late Dec	54 ± 21	68 ± 19	65 ± 27	50 ± 23
	Net heat input at water surface (W m^{-2})			
Early Dec	140 ± 17	147 ± 26	120 ± 22	137 ± 34
Mid-Dec	160 ± 12	169 ± 19	153 ± 14	165 ± 20
Late Dec	168 ± 12	173 ± 16	161 ± 15	169 ± 18

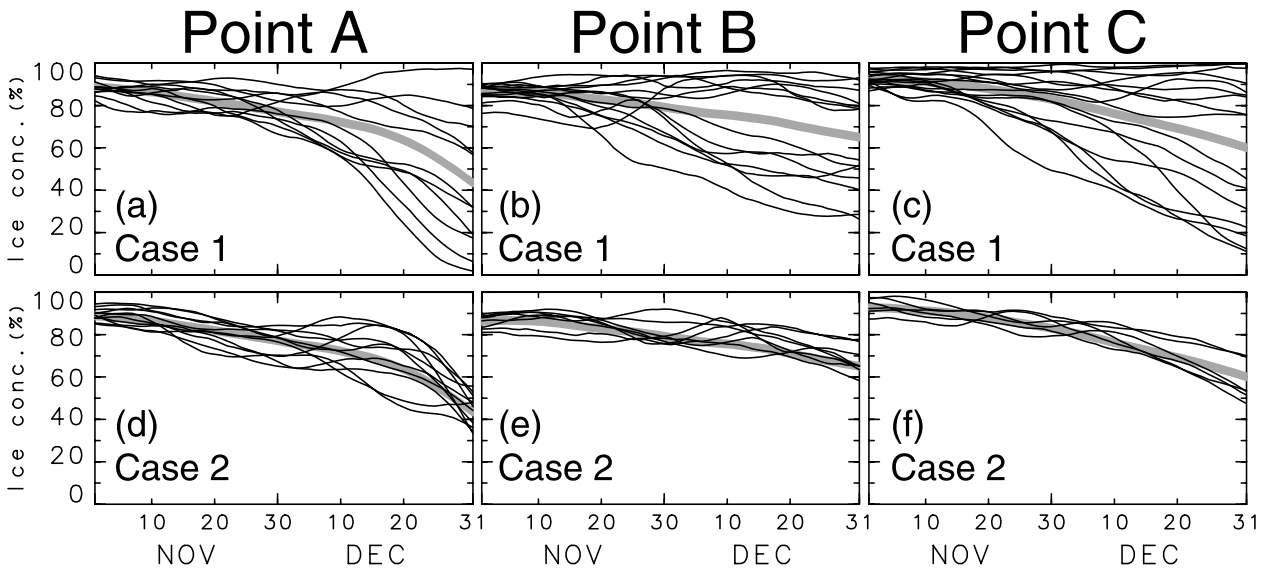

Figure 4. Categorized time series of daily ice concentration for (a–c) Case 1 and (d–f) Case 2 at points A–C. See text about the categorizations of Cases 1 and 2. The gray line indicates the 22-year climatological daily mean ice concentration at each point. The black line indicates ice concentration of each year. The daily ice concentration data have been smoothed using an 11-day running mean.

Ohshima and Nihashi, 2005]. Daily F_n values averaged over 22 years are used as model forcing (Figure 6a). The heat fluxes are calculated based on the formulae used by *Nihashi and Ohshima* [2001]. Specifically, the empirical formulae for the incoming shortwave and the longwave radiations are calculated according to *Zillman* [1972] and *Köenig-Langlo and Augstein* [1994], respectively. The turbulent heat fluxes are calculated from bulk formulae. We use the bulk transfer coefficients proposed by *Kondo* [1975], which incorporates the stability effect of the atmospheric surface layer. The model calculation starts after F_n becomes positive.

[26] Firstly, the time evolution of ice concentration C is calculated from the model (equations (B1) and (B2) in Appendix B) by giving initial ice concentration and initial water temperature (Figure 6b). The observed daily C averaged over 22 years is used as the initial C value. The initial water temperature is set to the freezing point. Eleven-day running means of F_n and observed C are used in the calculation because the focus is on the seasonal timescale. This experiment is hereafter defined as the 'basic run'. For comparison, observed climatological daily ice concentrations averaged for 22 years (Figure 4a) is also included in Figure 6b. The time evolutions of ice concentration obtained from the model agree well with the observed concentrations, suggesting the applicability of the model.

[27] The sensitivities of the model to the forcing and input parameters are determined by both doubling and halving these parameters. For the case of the basic run (Figure 6b), the sensitivities of the model ice concentration to F_n and h_0 are the largest ($\leq$40%) at the end of December, while the others are relatively small ($\leq$10%). Sea ice melts away at the end of December if F_n (h_0) is doubled (halved).

[28] Secondly, the model is used to intentionally increase or decrease 10% of the ice concentration as observed in late November (Figure 4a). The increase/decrease is done for 10 days in the middle of November. Here the change in ice concentration of 10% is assumed to be caused by the MID. The 10-day period is representative of the timescale for atmospheric disturbances. The results are presented in Figure 6b. The time evolutions of ice concentration by the model experiments are quite similar to the observations (Figures 4a and 5a). The difference between the basic run and the experiments increases 25–40% as sea ice melts from the end of November through the end of December (Figure 6c) as is also shown by the observa-

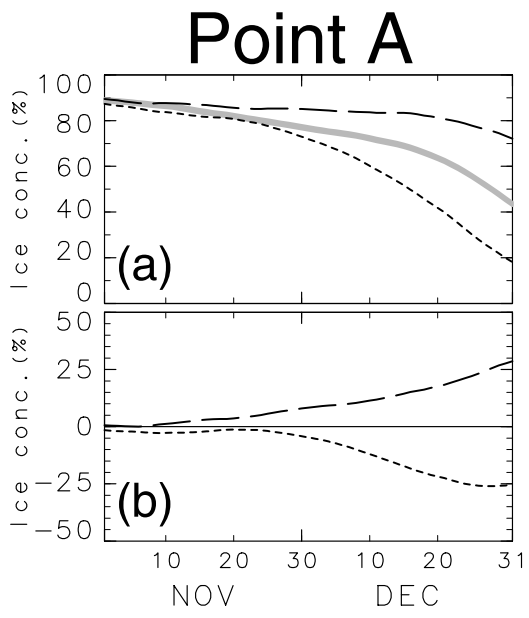

Figure 5. (a) Average time series for Case 1 at point A (Figure 4a). Dashed (dotted) line indicates the average of years that is larger (smaller) than the 22-year climatological daily mean ice concentration at point A (Figure 4a). (b) Differences between the climatology and the averages in Figure 5a. Dashed (dotted) line indicates the same case as in Figure 5a.

Table 2. Summary of Categorization (Cases 1 and 2) at Points A–D[a]

	Point A	Point B	Point C	Point D
Case 1	11	14	16	10
Case 2	11	8	6	12

[a]See text about the categorizations. The numbers denote years corresponding to each case.

tions (Figure 5b). Similar results are obtained at the other points (not shown here).

[29] For the case of the smaller ice concentration experiment (dotted line in Figure 6c), the increase of the difference becomes small when ice concentration is small as in the observational result (dotted line in Figure 5b). This is probably because the ratio of the heat used for sea-ice melt to the heat input decreases rapidly when ice concentration is small (More heat is used for increasing water temperature) [*Ohshima and Nihashi*, 2005]. Although the reliability of the model with constant ice thickness is weak in this situation when ice concentration is small (see Appendix B and *Ohshima and Nihashi* [2005]), the result that the ratio of the heat used for sea-ice melt to the heat input decreases rapidly is obtained even if the model had a variable ice thickness [*Ohshima and Nihashi*, 2005].

[30] Thirdly, a model experiment which excludes the ice–ocean albedo feedback is run. In this experiment, heat input into the upper ocean ($F_n(1-C)$ in equation (B1)) is assumed to be constant although the ice concentration can change. In other words, in this experiment the heat input into the upper ocean is only the constant heat flux from the deeper ocean (Q_o). Here Q_o is assumed to be 10 W m^{-2} following previous studies (see Introduction). The result is shown in Figure 6d. The ice concentration decreases almost linearly from the beginning of November (~90%) through the end of December (~70%). Now, one more experiment is done using the model with a different constant heat input. In this experiment, Q_o is increased to 40 W m^{-2} for 10 days in the middle of November (Figure 6d). The period of 10 days is the same as that of the experiments in Figure 6b. Here the change in Q_o can be assumed to be caused by the upwelling of the warm CDW due to the divergent wind field. A comparison of the results shown in Figures 5 and 6 indicate that the change in ice concentration and subsequent change in the heat input through open water do indeed result from the ice–ocean albedo feedback effect.

[31] The maps of correlation coefficients between the November MID and December ice concentration (Figures 2a and 2b) reveal that the correlations are generally positive in marginal ice zones, which contrasts with the negative correlations around the Antarctic continent. This dipole correlation pattern in the meridional direction is almost perfectly zonally symmetric around the Antarctic continent. The positive correlations are relatively weak when we compare the December MID and December ice concentration (Figure 2c). Also, from monthly maps of November MID anomalies (Figure 1a) and December ice concentration anomalies (Figure 1b), in the marginal ice zones, the positive/northward (negative/southward) MID anomaly areas tend to correspond to the positive (negative) ice concentration anomaly areas. The connection between ice drift and ice concentration in the marginal ice zone is indicated from analyses of the covariance between ice drift and ice concentration [*Venegas et al.*, 2001; *Venegas and Drinkwater*, 2001]; strong northward (southward) MID leads to anomalous northward (southward) ice extent. It

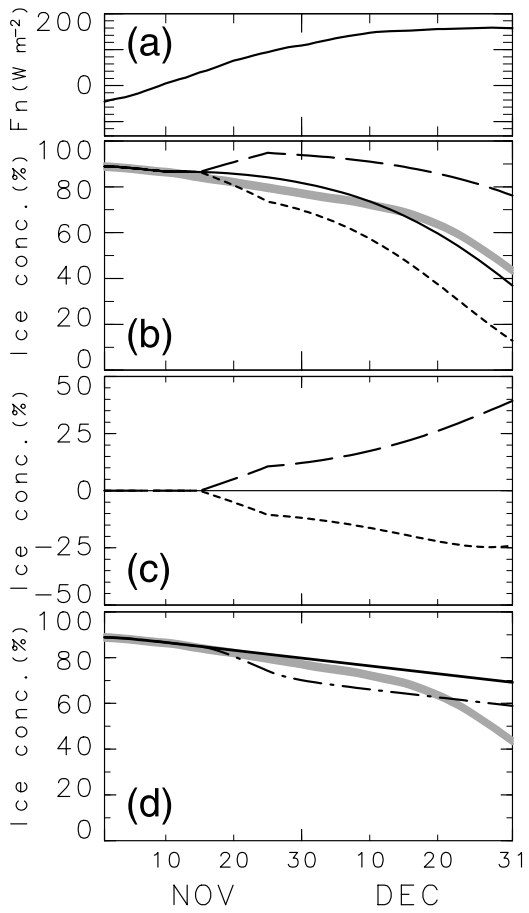

Figure 6. (a) Time series of the climatological daily net heat input at the water surface (F_n) at point A averaged from 1979 to 2001. The heat data has been smoothed using an 11-day running mean. (b) Time evolution of ice concentrations for point A, calculated from the ice–upper ocean coupled model. Black solid line indicates the result from the basic run. Dashed (dotted) line indicates an experiment in which we intentionally add (subtract) 10% of ice concentration for 10 days at the middle of November. Time series of the observed climatological daily ice concentration at point A (Figure 4a) are indicated by gray solid line. The daily ice concentration data have been smoothed using an 11-day running mean. (c) Differences between the basic run and the experiments (Figure 6b). Dashed (dotted) line indicates the same experiment as in Figure 6b. (d) Experiments in which the ice–ocean albedo feedback is excluded by assuming that heat input into the upper ocean is constant although the ice concentration can change. Black solid line indicates the experiment with a constant heat input of 10 W m^{-2}. Dash-dotted line indicates the experiment in which the constant heat input of 10 W m^{-2} is increased to 40 W m^{-2} for 10 days at the middle of November. Time series of the observed climatological daily ice concentration at point A (Figure 4a) are indicated by gray solid line.

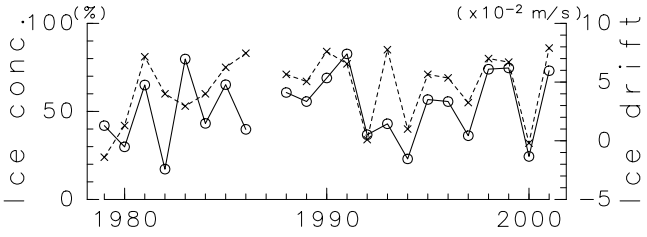

Figure 7. As in Figure 3, except for point D (Figure 2a).

was also found that synoptic variability in meridional winds determines ice-edge anomalies, which was shown from analyses of satellite derived ice concentration/motion data and meteorological data in the western Antarctic Peninsula region [*Stammerjohn et al.*, 2003]. Therefore, we argue that the marginal ice zone ice concentration anomalies in December are mainly determined by the November MID and that the ice concentration anomalies increase due to the ice–ocean albedo feedback effect.

[32] The same analyses as shown in Figures 3, 4, and 6 and in Tables 1 and 2 are made at the positive correlation grid point, point D in Figure 2a. The time series of the November MID and December ice concentration (Figure 7) shows that the MID and ice concentration change randomly during whole period (1979–2001) as in Figure 3. The time series of ice concentration (Figure 8 and Table 1) shows that the ice concentration anomaly increases toward the time of maximum melt as in Figure 4 and in Table 1. These results are consistent with those (not shown here) obtained using the simple ice–ocean coupled model described in Appendix B. The consistency of the observational and model results for the marginal ice zone strongly suggests the influence of an ice–ocean albedo feedback effect.

[33] The positive correlations in the marginal ice zone tend to be weaker than the negative correlations near Antarctica (Figures 2a and 2b). This is probably because a fixed continental boundary doesn't exist in the marginal ice zone and thus the relationship between ice drift and ice concentration is relatively weak. To reveal the cause of the initial ice concentration anomaly in the marginal ice zone, detailed ice motion data are needed to show the opening and closing of the ice pack. However, ice motions retrieved from satellite are unreliable during summer as we discussed in section 2. The other plausible reasons are the mixing of the upper ocean and a faster advection of upper ocean temperature anomalies in the marginal ice zone, although they are also difficult to show from available data.

[34] Somewhat weaker negative correlations are shown at about 64°S, 0°E (Figures 2a and 2b). The assumption that heat input mainly occurs at the water surface may not be valid in this region, because this area contains the Maud Rise where oceanic stratification is weak and thus heat entrained from the deeper ocean is expected to be large [*Gordon and Huber*, 1990].

[35] The net heat input into the ice–upper ocean system was assumed to be the product of the net heat input at water surface (F_n) and the open water fraction ($1-C$). In this study we ignored the interannual variation of F_n. The mean F_n and its standard deviation at points A–D calculated every 10 days during the active melt season (December) for the 22 years is included in Table 1. From this table, in mid-December, the interannual variation of heat input into the upper ocean caused by the anomaly in $1-C$, estimated as the product of the averaged F_n and the standard deviations in $1-C$, is from 4 to 8 times larger that that caused by the anomaly in F_n, estimated as the product of the averaged $1-C$ and the standard deviations in F_n. This indicates that interannual variation of heat input into the upper ocean is mainly determined by open water fraction.

[36] The accuracy of this study depends in part on the algorithm used to estimate ice concentrations from SMMR and SSM/I data. In this study we adopted the NASA Team (NT) algorithm. We have performed the same analysis using the Bootstrap algorithm [*Comiso*, 1995] which gives similar results (not shown here) to those of the NT algorithm. We also may need to pay attention to the effects of meltponds and wet snow on the estimation of ice concentrations from SMMR and SSM/I data. The presence of meltponds in the SMMR and SSM/I fields of view causes an underestimation of ice concentration. However, this effect is thought to be small in the Antarctic sea-ice zone because the meltpond area is very limited as described in the introduction. The presence of wet snow results in ice concentrations of 100% because wet snow behaves like a blackbody at microwave wavelengths. In the Ross Sea during summer, extensive flooding at the snow/ice interface due to heavy snow was observed, but there were no signs of meltponds or bare ice [*Morris and Jeffries*, 2001]. This wet snow may cause an overestimation of ice concentration particularly on daily time scales. For example, those cases where ice concentration increases in December (Figure 4) may be caused by this wet snow effect, although there is a possibility that this increase is caused by the advective effect of ice. However, these effects on our results are thought to be small because the ice concentration increases are not prominent in Figure 4.

5. Summary

[37] In this study we demonstrated an ice–ocean albedo feedback effect on sea-ice decay over the Antarctic sea-ice

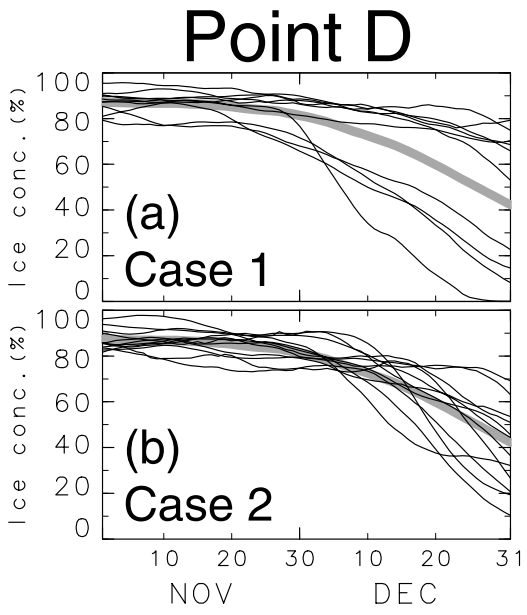

Figure 8. As in Figure 4, except for point D.

zone. Firstly, we made a comparison between November (beginning of the melt season) ice drift and December (active melt season) ice concentration because an initial anomaly in ice concentration is thought to be caused by ice drift. We mainly used ice drift calculated from SLP because the large-scale direct measurement of ice motion from satellites is problematic during late spring and summer due to rapid sea-ice decay and atmospheric effects. From the comparisons of ice drift from the satellites and that from SLP, it was shown that ice drift calculated from SLP provides a reliable distribution pattern of drift direction (Appendix A; Figure 9b), whereas the accuracy of the ice drift speed is relatively poor (Figure 9c). Therefore, we mainly focused on the coastal regions around Antarctica and used the meridional component of ice drift (MID) because the relationship between ice drift and ice concentration appears to be most robust: northward (southward) advection of ice will cause divergence (convergence) because of the influence of the fixed continental boundary. A map of correlation coefficients between the November MID calculated from SLP and December ice concentration for 22 years (Figure 2a) revealed that the correlations are generally negative around the Antarctic coast. A similar result was obtained when we used the November MID retrieved from the satellites (Figure 2b). The negative correlations around Antarctica between December MID and December ice concentration were relatively weak (Figure 2c), although the ice drift responds to winds instantaneously.

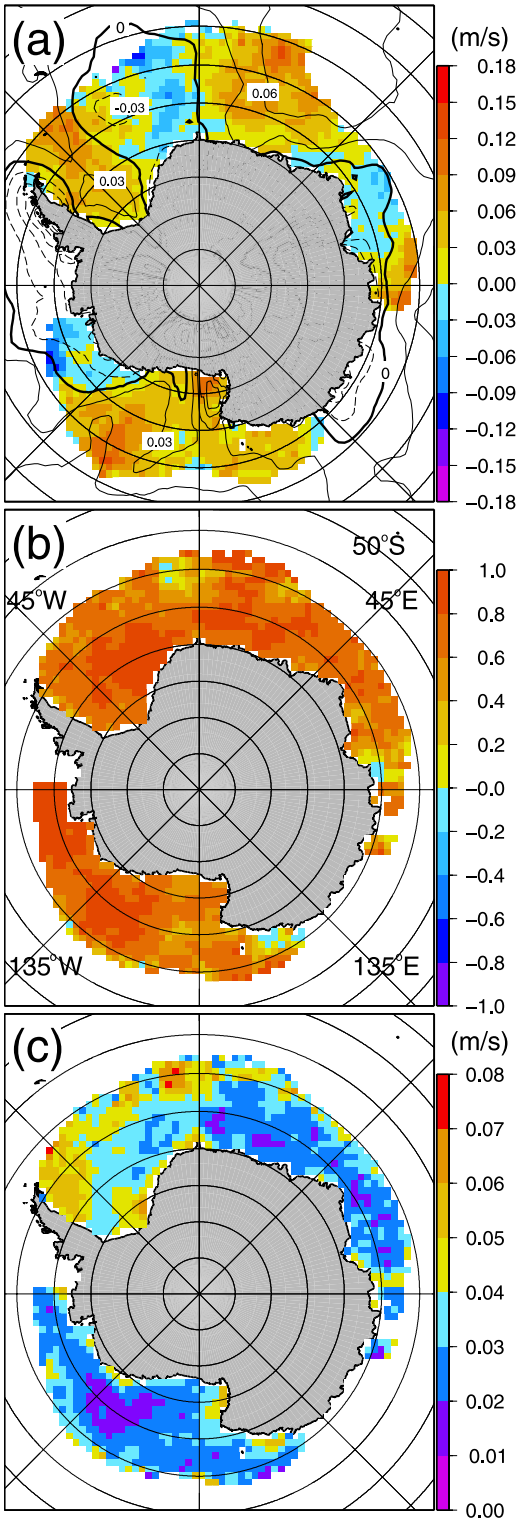

[38] Next, we made detailed analyses at grid points where the correlation coefficient is high. Time series of November MID and December ice concentration for 22 years (Figure 3) showed that they change randomly, implying that the high correlations in Figure 2a don't arise from a trend-like feature or periodic variation. Time series of observed ice concentration showed that ice concentration anomalies which appear at the beginning of the melt season increase toward the time of maximum melt (Table 1 and Figures 4a–4c and 5). This increase in ice concentration anomalies was also shown from the use of a simple ice–upper ocean coupled model which implicitly included an ice–ocean albedo feedback effect (Figures 6b and 6c). Thus, these results indicate the following ice–ocean albedo feedback effect: ice concentration anomalies initiated by wind at the beginning of the melt season lead to anomalous heat input through open water areas, and then the initial ice concentration anomalies increase through ice melting by the heat content of the upper ocean.

[39] Similar results were obtained for the marginal ice zone (Figures 7, 8, and Table 1) as in the coastal regions, although the correlations are positive (Figures 2a and 2c). Based on studies of the relationship between ice drift and ice concentration [*Venegas et al.*, 2001; *Venegas and Drinkwater*, 2001; *Stammerjohn et al.*, 2003], we argue that the MID causes an initial ice concentration anomaly which then increases through the ice–ocean albedo feedback effect. This effect holds true whether in the ice pack or in the marginal ice zone. For testing our assertion that the cause of the initial ice concentration anomaly is ice drift in

Figure 9. (a) Mean monthly meridional component of the ice drift (MID) calculated from SLP (shown by contours with a contour intervals of 0.03 m s^{-1}) and that retrieved from the satellite (shown by shading) for November 1988. MID derived from SLP is interpolated on the satellite derived ice motion grid. (b) Correlations coefficients between the November MID calculated from SLP and that retrieved from the satellites from 1979 to 1997. (c) Root mean squares of the difference between the November MID calculated from SLP and that retrieved from the satellites from 1979 to 1997.

the marginal ice zone where no fixed continental boundary exists, a high-resolution ice motion data set is needed. Further, the development of a detailed ice motion data set for the summer season will allow us to make a more quantitative analysis. Currently, ice motion retrievals from satellites are too unreliable during summer. The development and analysis of such a data set will be the subject of a future study.

[40] Finally, the mechanism of the ice–ocean albedo feedback effect may also explain, at least in part, the interannual variation of open water within the ice pack $(1-C)$ during spring (OND) and summer (JFM) as observed by *Zwally et al.* [2002]. From an analysis of the data used by Zwally et al., the largest standard deviation of open water areas occurs during the month of December. Through this ice–ocean albedo feedback mechanism, small ice concentration anomalies at the beginning of the melt season will increase and may explain in part the large interannual variability during the active melt season.

Appendix A: Comparison of Ice Drift Data

[41] In this appendix, the SLP-derived and satellite-derived mean meridional component of sea ice drift (MID) are compared. An example for November 1988 is shown in Figure 9a. The MID derived from SLP is interpolated onto the satellite derived ice motion grid using a Gaussian weighting function. From Figure 9a, we observe that the positive and negative MID patterns agree quite well with each other, except for the negative MID in the eastern Weddell Sea. Similar discrepancies have been found in some comparisons of ECMWF and NCEP SLP products with buoy and satellite derived ice drift data, which have been associated with errors in the computation of the surface pressure field by the model [*Drinkwater et al.*, 1999; *Stammerjohn et al.*, 2003]. On the other hand, a map of correlation coefficients between the November SLP-derived and satellite-derived MIDs for the entire period, 1979–1997, shows high positive correlations for most of the sea-ice zone (Figure 9b), indicating that the SLP errors are not very significant when comparisons are made for long (~20 years) periods.

[42] The root mean squares of the difference in speed between SLP-derived MID and satellite-derived MID are not small in the Weddell Sea, at the ice edge, and for the area adjacent to the coast (Figure 9c). In the Weddell Sea, relatively large discrepancies are shown. This is probably due to the Weddell Gyre [*Deacon*, 1979] because the oceanic current isn't included in the MID calculated from SLP. The discrepancies at the coastal regions and the ice edge are probably due to the effect of internal stress of ice.

[43] The findings from Figures 9b and 9c indicate that the MID positive and negative patterns as calculated from SLP are fairly reliable, but the accuracy of its speed is poor. For the case of the zonal component of the ice drift, similar results are obtained (not shown here).

Appendix B: A Simple Ice-Upper Ocean Model

[44] In this appendix, a simple ice–upper ocean coupled model for melting of the Antarctic sea ice proposed by *Ohshima and Nihashi* [2005] is briefly described. The model has an oceanic surface mixed layer with constant depth (H). The ice thickness h_0 is defined as the average thickness of individual floes comprising the ice medium and is assumed to be constant; and thus the ice melting is represented only by a decrease in ice concentration (C). Sea ice ablates through bottom and lateral melting of each ice floe or through breaking into smaller pieces and subsequent melting of brash ice. This model does not treat the melting of individual ice floes. The model considers this process in a bulk fashion and the meting is represented only by an overall areal change of sea ice since even bottom melting indirectly contributes to the areal change through making very thin ice that finally melts away.

[45] Heat input into the ice–upper ocean system is represented as the product of net heat input at the water surface (F_n) and open water fraction $(1-C)$. If sea-ice melting is caused by this heat input, the heat balance of the upper ocean is given by

$$c_w \rho_w H \frac{dT}{dt} = F_n(1-C) + L_f \rho_i h_0 \frac{dC}{dt}, \tag{B1}$$

where c_w (=3990 J kg^{-1} °C^{-1}) is the heat capacity of seawater; ρ_w(= 1026 kg m^{-3}) and ρ_i (= 900 kg m^{-3}) are the densities of seawater and sea ice, respectively; L_f is the latent heat of fusion for sea ice; and t is time. A fixed value of L_f = 0.276 MJ kg^{-1} corresponding to an observed salinity of 6 practical salinity unit (psu) is used. The melting rate of sea ice ($-L_f \rho_i h_0 \frac{dC}{dt}$) is assumed to be proportional to the difference between water temperature (T) and the freezing point ($T_f = -1.86$°C) and is parameterized as follows:

$$-L_f \rho_i h_0 \frac{dC}{dt} = c_w \rho_w K_b C(T - T_f), \tag{B2}$$

where K_b the bulk heat transfer coefficient between ice and ocean. The time evolution of ice concentration C can be obtained from equations (B1) and (B2) by giving model forcing (F_n), input parameters (H, h_0, and K_b), initial ice concentration, and initial water temperature.

[46] The assumption in this model that the average ice thickness is a constant might be too idealistic. The time evolution of ice concentration derived from a model incorporating ice thickness change following *Hibler* [1979] shows similar result in the ice concentration of 30–100%, while sea ice melts away faster when the concentration is <30% [*Ohshima and Nihashi*, 2005].

[47] **Acknowledgments.** The main part of this work was performed while S.N. held a National Research Council Research Associateship Award at NASA Goddard Space Flight Center. S.N. was also supported by RR2002 of Project for Sustainable Coexistence of Human, Nature and the Earth of the MEXT of the Japanese government. Suggestions and comments from three anonymous reviewers were very helpful. We thank Kay I. Ohshima for his comments on an early version of the manuscript.

References

Ackley, S. F., C. A. Geiger, J. C. King, E. C. Hunke, and J. Comiso (2001), The Ronne polynya of 1997–1998: Observations of air-ice-ocean interaction, *Ann. Glaciol.*, *33*, 425–429.

Andreas, E. L., and S. F. Ackley (1982), On the differences in ablation seasons of Arctic and Antarctic sea ice, *J. Atmos. Sci.*, *39*, 440–447.

Cavalieri, D. J., P. Gloersen, and W. J. Campbell (1984), Determination of sea ice parameters with the Nimbus 7 SMMR, *J. Geophys. Res.*, *89*, 5355–5369.

Cavalieri, D. J., J. Crawford, M. R. Drinkwater, D. Eppler, L. D. Farmer, R. R. Jentz, and C. C. Wackerman (1991), Aircraft active and passive microwave validation of sea ice concentration from the DMSP SSM/I, *J. Geophys. Res.*, *96*, 21,989–22,008.

Cavalieri, D. J., K. M. St. Germain, and C. T. Swift (1995), Reduction of weather effects in the calculation of sea ice concentration with the DMSP SSM/I, *J. Glaciol.*, *41*, 455–464.

Cavalieri, D., C. Parkinson, P. Gloersen, and H. J. Zwally (1999), Sea ice concentrations from Nimbus-7 SMMR and DMSP SSM/I passive microwave data [CD-ROM], Natl. Snow and Ice Data Cent., Boulder, Colo.

Comiso, J. C. (1995), SSM/I ice concentrations using the Bootstrap algorithm, *NASA Ref. Publ.*, *1380*, 40 pp.

Curry, J. A., J. L. Schramm, and E. E. Ebert (1995), Sea ice-albedo climate feedback mechanism, *J. Clim.*, *8*, 240–247.

Deacon, G. E. R. (1979), The Weddell gyre, *Deep Sea Res. Part A*, *26*, 981–995.

Drinkwater, M. R. (1998), Satellite microwave radar observation of Antarctic sea ice, in *Analysis of SAR Data of the Polar Oceans*, edited by C. Tsatsoulis and R. Kwok, pp. 145–187, Springer, New York.

Drinkwater, M. R., and X. Liu (1999), Active and passive microwave determination of the circulation and characteristics of Weddell and Ross sea ice, in *Proceedings of IGARSS'99*, *Rep. 99CH36293*, pp. 314–316, Inst. of Electr. and Electr. Eng., New York.

Drinkwater, M. R., and X. Liu (2000), Seasonal to interannual variability in Antarctic sea-ice surface melt, *IEEE Trans. Geosci. Remote Sens.*, *38*, 1827–1842.

Drinkwater, M. R., R. Kwok, C. A. Geiger, J. A. Maslanik, C. W. Flower, and W. J. Emery (1999), Quantifying surface fluxes in the ice-covered polar oceans using satellite microwave remote sensing data, paper presented at Ocean Observing System for Climate (OceanObs'99), Ocean Obs. Panel for Clim., San Raphael, France, 18–22 Oct.

Gleitz, M., U. V. Bathmann, and K. Kichte (1994), Build-up and decline of summer phytoplankton biomass in the eastern Weddell Sea, Antarctica, *Polar Biol.*, *14*, 413–422.

Gloersen, P., and D. J. Cavalieri (1986), Reduction of weather effects in the calculation of sea ice concentration from microwave radiances, *J. Geophys. Res.*, *91*, 3913–3919.

Gordon, A. L., and B. A. Huber (1990), Southern ocean winter mixed layer, *J. Geophys. Res.*, *95*, 11,655–11,672.

Hibler, W. D., III (1979), A dynamic thermodynamic sea-ice model, *J. Phys. Oceanogr.*, *9*, 815–846.

Hunke, E. C., and S. F. Ackley (2001), A numerical investigation of the 1997–1998 Ronne Polynya, *J. Geophys. Res.*, *106*, 22,373–22,382.

Köenig-Langlo, G., and E. Augstein (1994), Parameterization of the downward longwave radiation at the Earth's surface in polar regions, *Meteorol. Z. Neue Folge*, *3*, 343–347.

Kondo, J. (1975), Air-sea bulk transfer coefficient in diabatic conditions, *Boundary Layer Meteorol.*, *9*, 91–112.

Kottmeier, C., and L. Sellmann (1996), Atmospheric and oceanic forcing of Weddell Sea ice motion, *J. Geophys. Res.*, *101*, 20,809–20,824.

Kwok, R., A. Schweiger, D. A. Rothrock, S. Pang, and C. Kottmeier (1998), Sea ice motion from satellite passive microwave imagery assessed with ERS SAR and buoy motions, *J. Geophys. Res.*, *103*, 8191–8214.

Maykut, G. A., and M. G. McPhee (1995), Solar heating of the Arctic mixed layer, *J. Geophys. Res.*, *100*, 24,691–24,703.

Maykut, G. A., and D. K. Perovich (1987), The role of shortwave radiation in the summer decay of a sea ice cover, *J. Geophys. Res.*, *92*, 7032–7044.

McPhee, M. G., C. Kottmeier, and J. H. Morison (1999), Ocean heat flux in the central Weddell Sea during winter, *J. Phys. Oceanogr.*, *29*, 1166–1179.

Morris, K., and M. O. Jeffries (2001), Seasonal contrasts in snow cover characteristics on Ross Sea ice floes, *Ann. Glaciol.*, *33*, 61–68.

Nihashi, S., and K. I. Ohshima (2001), Relationship between the sea ice decay and solar heating through open water in the Antarctic sea ice zone, *J. Geophys. Res.*, *106*, 16,767–16,782.

Nihashi, S., K. I. Ohshima, M. O. Jeffries, and T. Kawamura (2005), Sea-ice melting processes inferred from ice-upper ocean relationships in the Ross Sea, Antarctica, *J. Geophys. Res.*, *110*, C02002, doi:10.1029/2003JC002235.

Ohshima, K. I., and S. Nihashi (2005), A simplified ice-ocean coupled model for melting of the Antarctic sea ice, *J. Phys. Oceanogr.*, *35*, 188–201.

Ohshima, K. I., K. Yoshida, H. Shimoda, M. Wakatsuchi, T. Endoh, and M. Fukuchi (1998), Relationship between the upper ocean and sea ice during the Antarctic melting season, *J. Geophys. Res.*, *103*, 7601–7615.

Schmitt, C., C. Kottmeier, S. Wassermann, and M. Drinkwater (2004), *Atlas of Antarctic Sea Ice Drift*, Univ. Karlsruhe, Karlsruhe, Germany.

Stammerjohn, S. E., M. R. Drinkwater, R. C. Smith, and X. Liu (2003), Ice-atmosphere interactions during sea-ice advance and retreat in the western Antarctic Peninsula region, *J. Geophys. Res.*, *108*(C10), 3329, doi:10.1029/2002JC001543.

Strass, V. H., and E. Fahrbach (1998), Temporal and regional variation of sea ice draft and coverage in the Weddell Sea obtained from upward looking sonars, in *Anterctic Sea Ice: Physical Processes, Interactions and Variability*, *Antarct. Res. Ser.*, vol. 74, edited by M. O. Jeffries, pp. 123–139, AGU, Washington, D. C.

Thorndike, A. S., and R. Colony (1982), Sea ice motion in response to geostrophic winds, *J. Geophys. Res.*, *87*, 5845–5852.

Timmermann, R., A. Worby, H. Goosse, and T. Fichefet (2004), Utilizing the ASPeCt sea ice thickness data set to evaluate a global coupled sea ice-ocean model, *J. Geophys. Res.*, *109*, C07017, doi:10.1029/2003JC002242.

Uotila, J., T. Vihma, and J. Laumiainen (2000), Response of the Weddell Sea pack ice to wind forcing, *J. Geophys. Res.*, *105*, 1135–1151.

Vaillancourt, R. D., R. N. Sambrotto, S. Green, and A. Matsuda (2003), Phytoplankton biomass and photosynthetic competency in the summertime Mertz Glacier region of East Antarctica, *Deep Sea Res., Part II*, *50*, 1415–1440.

Venegas, S. A., and M. R. Drinkwater (2001), Sea ice, atmosphere and upper ocean variability in the Weddell Sea, Antarctica, *J. Geophys. Res.*, *106*, 16,747–16,765.

Venegas, S., M. R. Drinkwater, and G. Shaffer (2001), Coupled oscillations in Antarctic sea ice and atmosphere in the Southern Pacific sector, *Geophys. Res. Lett.*, *28*, 3301–3304.

Vihma, T., J. Launiainen, and J. Uotila (1996), Weddell Sea ice drift: Kinematics and wind forcing, *J. Geophys. Res.*, *101*, 18,279–18,296.

White, W. B., and R. G. Peterson (1996), An Antarctic circumpolar wave in surface pressure, wind, temperature and sea-ice extent, *Nature*, *380*, 699–702.

Worby, A. P., R. A. Massom, I. Allison, V. I. Lytle, and P. Heil (1998), East Antarctic sea ice: A review of its structure, properties and drift, in *Anterctic Sea Ice: Physical Processes, Interactions and Variability*, *Antarct. Res. Ser.*, vol. 74, edited by M. O. Jeffries, pp. 41–67, AGU, Washington, D. C.

Zillman, J. W. (1972), A study of some aspects of the radiation and heat budgets of the southern hemisphere oceans, *Meteorol. Stud. 26*, 562 pp., Dep. of the Inter., Bur. of Meteorol., Canberra, Australia.

Zwally, H. J., J. C. Comiso, C. L. Parkinson, D. J. Cavalieri, and P. Gloersen (2002), Variability of Antarctic Sea Ice 1979–1998, *J. Geophys. Res.*, *107*(C5), 3041, doi:10.1029/2000JC000733.

D. J. Cavalieri, Hydrospheric and Biospheric Sciences Laboratory, NASA Goddard Space Flight Center, Greenbelt, MD 20771, USA.

S. Nihashi, Institute of Low Temperature Science, Hokkaido University, Sapporo 060-0819, Japan. (sohey@lowtem.hokudai.ac.jp)